Chaos, Solitons and Fractals 200 (2025) 117099

Contents lists available at ScienceDirect

Chaos, Solitons and Fractals

journal homepage: www.elsevier.com/locate/chaos

Unconventional tipping and wrinkled hysteresis loop in nonsmooth biophysical systems

Yoseb Kang [a], Sangil Kim [a], Ying-Cheng Lai [b,c], Younghae Do [d,*]

[a] Department of Mathematics, Institute for Future Earth, Pusan National University, Busan, 46241, Republic of Korea
[b] School of Electrical, Computer and Energy Engineering, Arizona State University, Tempe, 85287, USA
[c] Department of Physics, Arizona State University, Tempe, 85287, USA
[d] Department of Mathematics, Nonlinear Dynamics & Mathematical Application Center, Kyungpook National University, Daegu, 41566, Republic of Korea

ARTICLE INFO

Keywords:
Tipping point
Scaling law
Atopic dermatitis

ABSTRACT

A tipping point in nonlinear dynamical systems was previously understood as an abrupt transition from a high to a low stable steady state as a bifurcation parameter crosses a critical value. We uncover an unconventional tipping phenomenon in a class of non-autonomous nonsmooth biophysical systems, where the transition occurs through an intermediate, oscillatory state. Such a "stepping-stone" state also occurs in the reverse process of recovery, resulting in a "wrinkled" hysteresis loop. The dwelling time in the oscillatory state, e.g., the transient tipping time before the system settles in the low steady state, depends on the rate of the parameter change. The scaling laws of the transient tipping and recovery times are derived analytically. The intermediate state presents an opportunity for control intervention to prevent a healthy system from collapsing into a diseased state.

1. Introduction

The past half century has witnessed an increasing utilization of nonlinear dynamics to understand various diseases [1,2], where the central idea is that diseases are the result of some critical transition or tipping in the underlying physiological dynamical system [3,4], leading to the concept of dynamical diseases [5]. Methodologies in nonlinear dynamics that have been exploited to understand dynamical diseases such as epilepsy [6,7] include the Lyapunov exponents [8,9], the correlation dimension [10], and phase synchronization [11]. The focus of this paper is on tipping in a major class of human skin diseases: atopic dermatitis (AD) - a prevalent skin condition [12,13] governed by the complex interplay among genetic, immunological, and environmental factors [14] with diverse phenotypes and endophenotypes [15] as well as regional and age-related differences in AD clinical characteristics [16]. While being common, the manifestations of AD vary drastically across age groups, ethnicity, and genders, making it difficult to develop universally effective methods of treatment. For example, in the age group from birth to seven years old [17], AD is often associated with asthma [18]. It was also found that the AD phenotypes depends on the timing of onset and progression in childhood [19]. In adults with acute AD, the cytokine levels were found to be related to the SCORAD index [20]. Because of the diversity in the AD manifestations and courses of evolution [21], it has been challenging to understand its mechanism and long-term evolution [22] so as to develop universally applicable treatment. The rarity of robust animal models further complicates the translation of theoretical research into clinical practice. Recently, the focus has shifted towards *in vivo*, *in vitro*, and *in silico* methods to dissect the pathophysiological underpinnings of AD and to identify critical therapeutic targets and biomarkers, where

* Corresponding author.
E-mail address: yhdo@knu.ac.kr (Y. Do).

https://doi.org/10.1016/j.chaos.2025.117099
Received 7 May 2025; Received in revised form 14 July 2025; Accepted 18 August 2025
Available online 27 August 2025

mathematical modeling [23] and computational analysis are playing an increasing role [24]. More specifically, a computational design of treatment strategies for proactive therapy on AD using optimal control theory was developed [25]. Mathematical modeling of AD revealed "double-switch" mechanisms underlying four common disease phenotypes [26], a bifurcation analysis was developed to determine patient-specific effects of treatments on dynamic phenotypes [27], and multistability [28] and complex transient dynamics [29] in the AD model was investigated [28]. From the point of view of dynamics, the AD systems are nonsmooth because of the various biological switches involved [26]. As will be demonstrated and explained, because of the non-smoothness, the tipping phenomenon exhibits unique features that are not seen in smooth dynamical systems.

The broad phenomenon of tipping in dynamical systems has been understood as a sudden transition from one stable steady state to another as a bifurcation parameter changes through a critical point. Such systems are bistable and, as the parameter reverses its change, a transition to the original steady state can occur but at a parameter value differing from the tipping point, leading to a hysteresis loop that is quite common in bistable physical and biological systems.

For example, in biology, multistability, bifurcations, and hysteresis were studied in a large class of biological positive-feedback systems [30] and robust bistable patterning was discovered on the dorsal surface of the Drosophila embryo [31]. In systems biology, multistability was found to play a key role in regulated stochastic cell fate determination [32], control of gene regulatory networks [33], and the engineering of a synthetic quadrastable gene network on Waddington landscape for cell fate [34]. In optics, bistability was discovered in nonlinear plasmonic cloaks to realize giant all-optical scattering switching [35], in an atomic coherent medium [36], and in all-microwave switching [37]. In nanomagnetics, multistable free states of an active particle was discovered in coherent memory dynamics [38] and in magnetoelastic switching of non-ideal nanomagnets with defects [39]. Moreover, a class of mesoscopic superconducting memory based on bistable magnetic textures was studied [40]. Quite recently, folding states within a hysteresis loop as a hidden form of multistability were discovered in a number of nonlinear physical systems [41].

A field in which tipping is of particular interest is ecological systems where bistability is ubiquitous [42]. For example, in a shallow lake, two contrasting stable states can coexist: a clear-water state dominated by aquatic plants and a turbid-water state with excessive algae and suspended sediment [43]. Early-warning signals for critical transitions between two coexisting stable states (or tipping [44]) in ecological systems were studied [45] and the need to forecast tipping points was emphasized [46]. In certain ecological systems, regime shifts can occur without warning [47] and early warning signals of extinction in deteriorating environments were discovered [48]. The limits to detection of early warning for critical transitions in ecosystems were quantified [49], and generic indicators for loss of resilience before a tipping point leading to population collapse were uncovered [50]. Tipping points in ecological networks were discovered [51]. It was also found that the sudden collapse of pollinator communities can be attributed to tipping [52]. Tipping in macroeconomic agent-based models [53] was uncovered. In complex mutualistic networks of plants and pollinators, predicting tipping through dimension reduction was studied [54] and a control strategy was articulated to prevent tipping [55]. In these ecological networks, noise was found to play a beneficial role in species recovery [56] and control [57], and transient dynamics can arise due to noise [58]. Multiplexity in mutualistic networks can also be exploited to mitigate tipping [59]. (A comprehensive review of bistability and tipping in ecosystems is available [60].)

Bistability and tipping also arise in other fields. For example, in medicine, early-warning signals were proposed for detecting sudden deterioration of complex diseases through dynamical network biomarkers [61], and such biomarkers can be effective indicators of pulmonary metastasis at the tipping point of hepatocellular carcinoma [62]. In climate science, tipping may be predicted as a noisy bifurcation [63], there can be noise-induced and rate-dependent tipping events in climate systems [64], and critical slowing down can be used for early warning of tipping [65]. It was argued that a state shift may be occurring in Earth's biosphere [66]. A stochastic integrated assessment of the climate tipping points indicated the need for strict climate policy [67]. A significant example where global climate change makes tipping significantly more likely in critical natural systems is the Atlantic Meridional Overturning Circulation (AMOC) [68], which supports livable temperature conditions in Western Europe [69]. The evolution of the AMOC since 1980 was studied [70] and the risk of tipping the overturning circulation due to increasing rates of ice melt was pointed out [71]. Recently, model-based statistical [72] and data-driven machine learning [73] methods were recently developed to predict the potential tipping or collapse of the AMOC.

In general, nonautonomous dynamical systems with some time-dependent bifurcation parameter are vulnerable to tipping as it can be triggered by the time-rate change of the parameter, the phenomenon of rate-induced tipping [64]. Bifurcation and rate-induced tipping caused by parameter shifts in low-dimensional nonautonomous systems was studied [74]. Rate-induced tipping in a predator–prey system was discovered [75] and the rate of environmental change as an important driver across scales in ecology was noted [76]. It was also found that rate-induced tipping can trigger plankton blooms [77]. The dynamical mechanism of rate-induced tipping [78] from the perspective of global phase space was elucidated [79]. In most existing studies on tipping, the transition is typically abrupt through a saddle–node type of bifurcation.

In this paper, we present a phenomenon in nonsmooth dynamical systems where tipping occurs in an unconventional manner that is characteristically different from any known scenario. In particular, the system still possesses two stable steady states. As a bifurcation parameter changes with time (thereby making the system nonautonomous), a transition from one stable steady state to another eventually occur, but through a "stepping-stone" type of intermediate attractor that is not a steady state but oscillatory. As illustrated in Fig. 1, at the first critical point, denoted as q_1, a transition from the high stable state to the intermediate attractor occurs, followed by a transition from this attractor to the low steady state at q_2. Likewise, in the reverse process of recovery, the system moves out of the low steady state to a different intermediate attractor at q_3, and the subsequent transition from this attractor to the high steady state at q_4 completes the hysteresis loop. While the two stable steady states do not depend on how fast the parameter changes, the intermediate attractor does depend on the time rate change of the parameter. To our knowledge, hysteresis loops in physical and biological systems reported in the literature are typically associated with abrupt but nonetheless smooth transitions between the two stable steady states, as described in the preceding paragraphs. However, in our case, the loop becomes irregular and "wrinkled" due to the system's wandering on an oscillatory attractor before finally approaching a stable steady state. The dwelling or the transient time in the oscillatory state depends on the rate of parameter change and exhibits an algebraic scaling behavior, which can be understood analytically.

2. Nonlinear dynamics of atopic dermatitis

2.1. Mathematical model of AD

The biophysical mechanism of AD pathogenesis progression is captured by the model [26] in Fig. 1(a), as governed by the interactions between the skin barrier, immune regulation, and environmental stress. Under normal conditions, small amounts of pathogens entering through compromised skin barriers are naturally contained and pose no significant threat. However, when the pathogen load exceeds a threshold, a critical point is reached, at which physiological switches R and K are activated, such as toll-like receptors and protease-activated receptor 2. As a result, an AD flare is triggered. The immune response includes the release of antimicrobial peptides that combat the invading pathogens and signal various immune mechanisms that mobilize dendritic cells to the lymph nodes. If the pathogen level decreases below a deactivation threshold, these switches are turned off, stopping the AD flare. Conversely, if the dendritic cell count in the lymph nodes surpasses a second critical threshold, a further, irreversible change (G switch) in the immune state occurs, exacerbating the skin condition. Because of the activation and deactivation of the switches, the underlying dynamical system is nonsmooth. Quantitatively, the AD mechanism can be described by the following set of nonlinear differential equations:

$$\begin{aligned}
\frac{dP}{dt} &= \frac{P_{\rm env}\kappa_p}{1+\gamma_B B(t)} - \alpha_I R(t)P(t) - \delta_p P(t),\\
\frac{dB}{dt} &= \frac{\kappa_B[1-B(t)]}{[1+\gamma_R R(t)][1+\gamma_G G(t)]} - \delta_B K(t)B(t),\\
\frac{dD}{dt} &= \kappa_D R(t) - \delta_D D(t),
\end{aligned} \tag{1}$$

where $P(t) \geq 0$, $0 \leq B(t) \leq 1$ and $D(t) \geq 0$ denote the infiltrated pathogen load (in milligrams per milliliter), the strength of barrier integrity (relative to the maximum strength), and the concentration of dendritic cells in the lymph node (cells per milliliter), respectively. The typical parameter values are listed in Appendix A.

The structure of the skin barrier is dependent on the proteins keratin and filaggrin (FLG), and the extracellular matrix containing lipids, structural proteins, and the serine protease subgroup kallikreins. Dysfunction of these components can result in barrier defects, as typically found in loss-of-function mutations of the FLG gene [80]. The AD model (1) utilizes switches to describe the activation of the immune system, as shown in Fig. 1(a). In particular, the switches $R(t)$, $G(t)$ and $K(t)$ [26] depict the levels of activated immune receptors, *Gata*3 transcription relative to the maximum transcription level, and active kallikreins, respectively, which are given by

$$R(t) = \begin{cases} R_{\rm off}, & \text{for } P(t) < P^- \text{ or} \\ & \{P^- \leq P(t) \leq P^+,\ R(t^-) = R_{\rm off}\}, \\ R_{\rm on}, & \text{for } P(t) > P^+ \text{ or} \\ & \{P^- \leq P(t) \leq P^+,\ R(t^-) = R_{\rm on}\}, \end{cases} \tag{2}$$

$$K(t) = \begin{cases} K_{\rm off}, & \text{for } P(t) < P^- \text{ or} \\ & \{P^- \leq P(t) \leq P^+,\ R(t^-) = R_{\rm off}\}, \\ m_{\rm on}P(t) - \beta_{\rm on}, & \text{for } P(t) > P^+ \text{ or} \\ & \{P^- \leq P(t) \leq P^+,\ R(t^-) = R_{\rm on}\}, \end{cases} \tag{3}$$

$$G(t) = \begin{cases} G_{\rm off}, & \text{for } D(t) < D^+ \text{ and } G(t^-) = G_{\rm off}, \\ G_{\rm on}, & \text{for } D(t) \geq D^+ \text{ or } G(t^-) = G_{\rm on}, \end{cases} \tag{4}$$

where $R_{\rm on}$, $R_{\rm off}$, $G_{\rm on}$, $G_{\rm off}$ and $K_{\rm off}$ are parameters characterizing the activating or inactivating constant-level of the switches, but $K_{\rm on}$ depends on $P(t)$: $K_{\rm on} = m_{\rm on}P(t) - \beta_{\rm on}$, and the two switches R and K work together simultaneously.

Note that the switches R and K are hysteretic, which activate and cease AD flares. In contrast, switch G is irreversible: once activated, it remains on.

2.2. Bifurcation of AD dynamics

The AD system (1) exhibits complicated dynamical phenomena including multistability, transients and nonsmooth bifurcations [28,29]. Previous works [26,28] revealed four distinct attractors corresponding to the four stages of AD: healthy recovery (H), chronic damage (C), mild oscillations (O_m), and severe oscillations (O_s). Fig. 1(b) illustrates that the two steady-state attractors, labeled as H and C, do not exhibit any oscillatory behavior. Specifically, the skin integrity level is represented by $B = 1$ for the healthy skin state (H) and $B = 0$ for severe skin damage (C). In contrast, the oscillatory attractors, O_m and O_s, display fluctuating

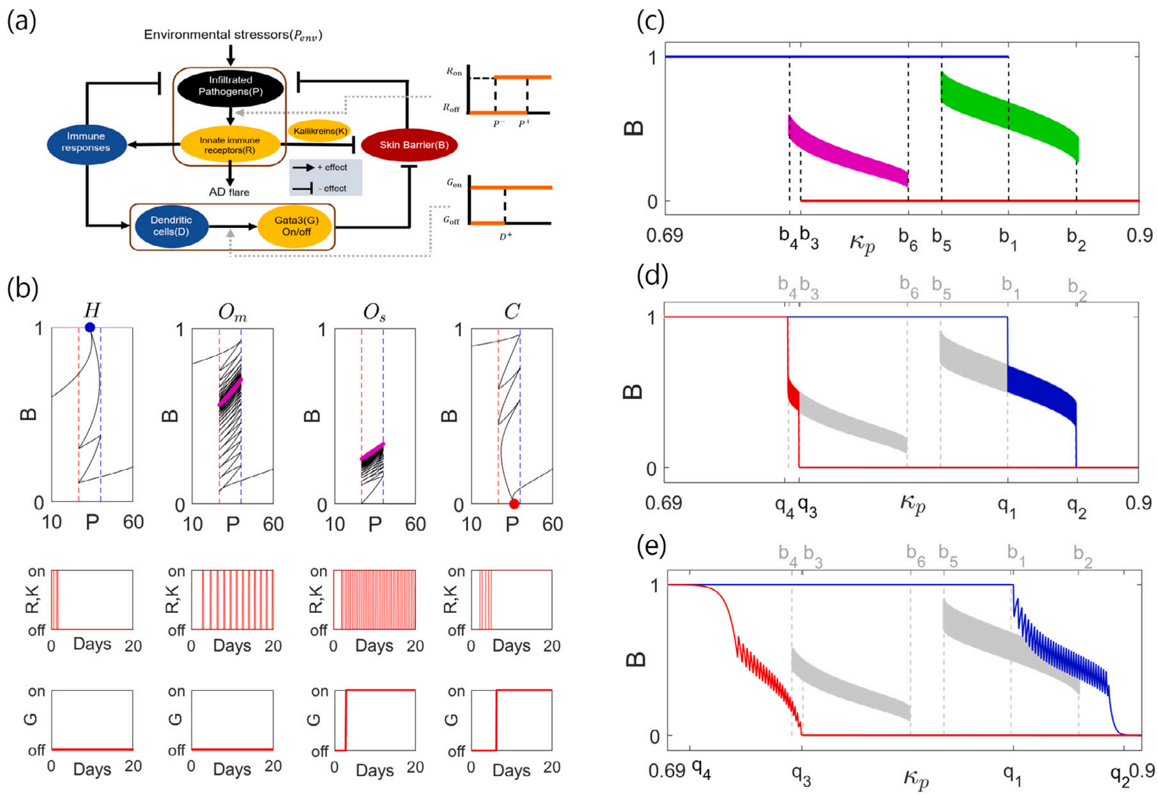

Fig. 1. AD system, unconventional tipping and wrinkled hysteresis loop. (a) The biophysical processes underlying AD leading to a nonsmooth dynamical system. (b) Behavior of four attractors over time, illustrating the activation and inactivation of the R, K-switch, as well as the activation of the G-switch. (c) A bifurcation diagram with the nominal skin permeability κ_p, revealing multiple coexisting attractors. There are a low stable steady state $B = 0$ (red, denoted as C), a high stable steady state $B = 1$ (blue, H), and two oscillatory attractors in between (O_s - purple and O_m - green). The rate of pathogen eradication is fixed at $\alpha_I = 0.1$. There are six distinct bifurcation points b_i ($i = 1, \ldots, 6$). At each point, either a new attractor emerges or an existing attractor disappears. (d) For the corresponding nonautonomous system with $\kappa_p(t) = \kappa_p^s + \epsilon t$ ($\epsilon = 10^{-6}$), unconventional tipping occurs, where the system transits from H to O_m at $\kappa_p = q_1$, followed by another transition to C at q_2. The reverse process is also through two transitions: one at q_3 and another at q_4. The gray background marks the oscillatory attractors in (c). As a result of the four transitions, the hysteresis loop becomes wrinkled. (e) Similar transitions and wrinkled hysteresis loop for $\epsilon = 10^{-3}$. (For interpretation of the references to color in this figure legend, the reader is referred to the web version of this article.)

behavior in skin integrity, highlighting the dynamic progression of AD. A key distinction between these two oscillatory attractors is the activation of the G switch: the G switch for O_m remains consistently off, while for O_s, it remains consistently on, as shown in Fig. 1(b). Two key parameters are the nominal skin permeability κ_p and the rate α_I of pathogen eradication. One dynamic feature observed in the AD system is multistability. For example, with a fixed parameter pair $(\kappa_p, \alpha_I) = (0.835, 0.114)$ in this region, the steady-state attractors H, O_m, O_s, and C can all emerge due to multistability [28]. This means that, depending on the initial conditions, any of these attractors can occur [28].

Fig. 1(c) shows a typical bifurcation diagram with κ_p for $\alpha_I = 0.1$, where there are six distinct bifurcation points b_i ($i = 1, \ldots, 6$) with four attractors in different parameter intervals. In particular, for $\kappa_p < b_4$, the high steady state, denoted as H and represented in blue, is the only attractor. As κ_p increases through b_4, the attractor O_s, represented by purple, emerges. For $b_4 \leq \kappa_p \leq b_3$, the system has two coexisting attractors, signifying bistability. At $\kappa_p = b_3$, a low steady state attractor, denoted as C and represented in red, is born. For $b_3 \leq \kappa_p \leq b_6$, the system has three coexisting attractors, leading to multistability. At b_6, O_s is destroyed and the system has two coexisting steady-state attractors for $b_6 \leq \kappa_p \leq b_5$. At b_5, the mild oscillatory attractor O_m, represented in green, is created and the system has three coexisting attractors again for $b_5 \leq \kappa_p \leq b_1$. At b_1 and b_2, respectively, the high steady state (H) and the mild oscillatory attractor (O_m) disappear, respectively, and the system has two coexisting attractors for $b_1 \leq \kappa_p \leq b_2$. For $\kappa_p > b_2$, the low steady state (C) is the only attractor.

That is, by varying κ_p, the number of existing attractors changes in the following sequence: $1 \to 2 \to 3 \to 2 \to 3 \to 2 \to 1$. This unique bifurcation behavior, as illustrated in Fig. 1(b), can only be observed in nonsmooth dynamical systems, making it a characteristic feature of such systems. Recent studies have examined the frequency characteristics of oscillatory states, O_m and O_s, in relation to inflammation dynamics of AD [81]. In general, the bifurcation at the tipping point belongs to the type of boundary equilibrium bifurcations [27].

Note that κ_p characterizes the skin condition, where large values of κ_p correspond to a more deteriorated condition. For $\kappa_p < b_4$, patient's skin condition is healthy, where the high steady state is the only attractor in the system. As κ_p increases through b_4, clinic symptoms of varying degrees as characterized by the occurrence of the oscillatory attractors and the low steady state. For $\kappa_p > b_2$, AD has evolved into the most severe stage.

3. Results

The AD system (1) is nonautonomous as the skin condition changes with time for a variety of reasons including aging. To model this feature, we set the nominal skin permeability as a function of time [82,83]:

$$\kappa_p(t) = \kappa_p^s \pm \epsilon t, \tag{5}$$

where κ_p^s is the initial value and ϵ is the linear ramping rate. The forward (+) and backward (−) conditions indicate that the skin condition will deteriorate and improve with time, respectively.

We fix the initial value κ_p^s at 0.69 for the forward direction and 0.9 for the backward direction. Fig. 1(d) shows, for $\epsilon = 10^{-6}$, forward (backward) trajectories. As the skin conditions deteriorate, a tipping transition occurs in the relative strength $B(t)$ of the barrier integrity at q_1 from the high steady state to the oscillatory state O_m (the blue trajectory, corresponding to mild skin disease). The system remains in O_m until κ_p reaches the second critical point $q_2 > q_1$, at which $B(t)$ drops to near zero, signifying reaching the most severe stage of AD. For reference, the bifurcation diagram in Fig. 1(c) for the autonomous system is included in Fig. 1(d) as the gray background. In the nonautonomous system, both transitions at q_1 and q_2 are abrupt, which is characteristic of tipping. Overall, the tipping from the high healthy state to the intermediate oscillatory state, the system's maintaining in this state for a finite parameter interval (equivalently, a finite amount of time) and the second tipping to the low steady state, constitute an unconventional, two-stage tipping transition. This makes the tipping branch of the hysteresis loop rippled, in contrast to the tipping behavior directly from the high to the low stable steady state in smooth dynamical systems.

A similar phenomenon occurs in the backward direction of the parameter variation: $\kappa_p(t) = \kappa_p^s - \epsilon t$, where the skin condition is improved. At the transition point $q_3 < q_1$, a sudden transition from the low steady state to another intermediate oscillatory state, O_s, occurs. The system stays in O_s for a finite parameter interval (time) before an abrupt transition back to the high stable steady state at $q_4 < q_3$. Owing to the dwelling in the oscillatory state O_s, the recovery process from the low to the high steady state is also unconventional, contributing to an irregular branch of the hysteresis loop. Compared with a typical hysteresis loop in smooth dynamical systems, the overall hysteresis loop represented by the blue and red curves in Fig. 1(d) is "wrinkled".

Two remarks are in order. First, in the nonautonomous AD system, the tipping points q_i are different from the corresponding bifurcating points b_i in the autonomous system, as indicated in Fig. 1(d). This difference can be understood analytically (see Appendices B and C). Second, the phenomena of unconventional tipping and wrinkled hysteresis loop can occur for different time rate change of the bifurcation parameter, as exemplified in Fig. 1(e) for $\epsilon = 10^{-3}$, a rate that is three orders of magnitude higher than that in Fig. 1(d). The initial values κ_p^s for the forward and backward trajectories, as shown in Fig. 1(e), are 0.69 and 0.90, respectively. At this rate, the first tipping occurs at approximately the same point q_1 but the oscillatory state of mild AD lasts in a larger parameter interval as a higher critical value q_2 is required for the system to switch to the low steady state associated with severe AD. Likewise, while the first recovery point q_3 in Figs. 1(d) and 1(e) are approximately the same, the oscillatory state lasts through a larger parameter interval and the skin condition as characterized by the value of κ_p needs to be significantly more improved for a full recovery at $\epsilon = 10^{-3}$ than at $\epsilon = 10^{-6}$. In fact, the quantities $q_i - b_i$ $(i = 1, 2, 3, 4)$, the differences between the transition points in the nonautonomous system and their corresponding bifurcation points in the autonomous system, depend on the rate ϵ and obey scaling laws. In spite of the differences in the detailed transitions, the tipping and recovery transitions contain multiple stages through some oscillatory state as the "springboard" and the overall hysteresis loop remains wrinkled.

The unconventional, two-stage tipping process in the AD system, as demonstrated in Figs. 1(d) and 1(e), is drastically different from conventional tipping in smooth dynamical systems. To better appreciate the difference, we note that, in a nonautonomous smooth system, tipping occurs almost instantaneously: due to the little parameter change required at the critical point for tipping, practically it takes an infinitesimal amount time for the transition from the high to the low stable steady state to occur. However, in the nonsmooth AD system, the time for tipping, or the transient tipping time between the two consecutive tipping points denoted as τ_{tp}, to occur can be quite long. Figs. 2(a) and 2(b) show, for $\epsilon = 10^{-6}$ and 10^{-3}, respectively, the length of the transient tipping time, where the difference in the transient time in the two cases is about three orders of magnitude (approximately 10 times larger than the difference in the parameter ramping rate). Similarly, the recovery process also involves a long transient process, as illustrated in Figs. 2(c) and 2(d).

To characterize unconventional tipping and the wrinkled hysteresis loop, we examine four quantities: (1) the tipping parameter interval $(\Delta q)_{\mathrm{tp}} \equiv q_2 - q_1$ [cf., Figs. 1(d, e)] (2) the recovery parameter interval $(\Delta q)_{\mathrm{rc}} \equiv q_3 - q_4$ [cf., Figs. 1(d, e)], (3) the transient tipping time τ_{tp} [cf., Figs. 2(a, b)] and (4) the transient recovery time τ_{rc} [cf., Figs. 2(c, d)]. As these quantities depend on the parameter ramping rate ϵ, we ask what scaling relations between them and ϵ are. Figs. 3(a) and 3(b) show the numerically obtained representative scaling behavior of $(\Delta q)_{\mathrm{tp}}(\epsilon)$ and $(\Delta q)_{\mathrm{rc}}(\epsilon)$, respectively. For a slow rate $\epsilon \ll \epsilon_c$, $(\Delta q)_{\mathrm{tp}}(\epsilon)$ and $(\Delta q)_{\mathrm{rc}}(\epsilon)$ approach the parameter difference between the two static bifurcation points, $b_2 - b_1$ and $b_3 - b_4$, respectively. However, for $\epsilon \gg \epsilon_c$, $(\Delta q)_{\mathrm{tp}}(\epsilon)$ and $(\Delta q)_{\mathrm{rc}}(\epsilon)$ increase algebraically with ϵ, with the respective scaling exponent $\beta_{\mathrm{tp}} \approx 0.63$ and $\beta_{\mathrm{rc}} \approx 1$. We have

$$(\Delta q)_{\mathrm{tp}}(\epsilon) \sim \begin{cases} \epsilon^{\beta_{\mathrm{tp}}} & \epsilon > \epsilon_c, \\ b_2 - b_1 & \epsilon < \epsilon_c, \end{cases} \tag{6}$$

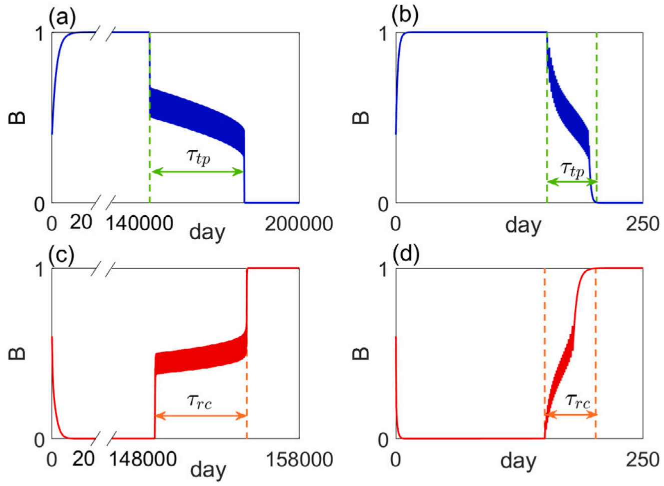

Fig. 2. Transient tipping and recovery process. (a, b) A relatively long and short transient process for the tipping from the high to low stable state to finish for $\epsilon = 10^{-6}$ and 10^{-3}. respectively. (c, d) Similar transient recovery process for $\epsilon = 10^{-6}$ and 10^{-3}, respectively. For the two values of the ramping rate, the difference in the transient time is more than the time difference as determined by the rate.

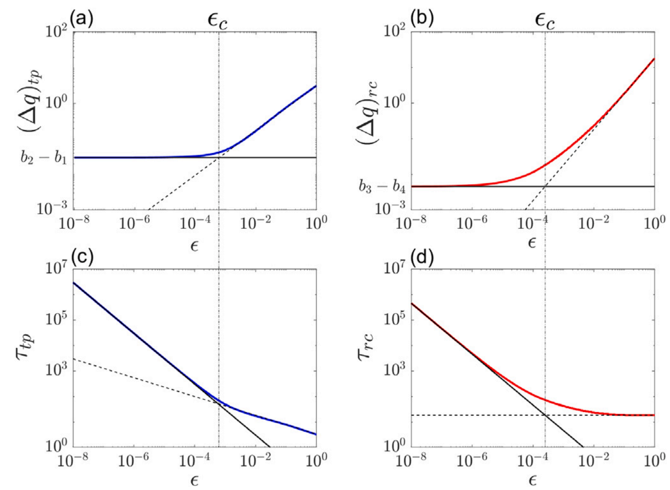

Fig. 3. Scaling of tipping and recovery parameter intervals, and of the transient tipping and recovery times with the parameter ramping rate. (a, b) Scaling of $(\Delta q)_{\rm tp}(\epsilon)$ and $(\Delta q)_{\rm rc}(\epsilon)$, respectively. The two horizontal asymptotic solid lines correspond to the difference between the two consecutive bifurcation points, i.e., $b_2 - b_1$ and $b_3 - b_4$, respectively. (c, d) Scaling of $\tau_{\rm tp}(\epsilon)$ and $\tau_{\rm rc}(\epsilon)$, respectively, where ϵ_c is determined by the intersection of the dashed and solid black lines, representing the asymptotic lines of two scaling curves in log–log scale. Here, ϵ_c is given by 6×10^{-4} and 2.5×10^{-4} for the forward and backward directions, respectively. (For interpretation of the references to color in this figure legend, the reader is referred to the web version of this article.)

$$(\Delta q)_{\rm rc}(\epsilon) \sim \begin{cases} \epsilon^{\beta_{\rm rc}} & \epsilon > \epsilon_c, \\ b_3 - b_4 & \epsilon < \epsilon_c. \end{cases} \tag{7}$$

These scaling results indicate that, for a more rapid change of the parameter, both the tipping and recovery processes require a larger parameter change to complete. The scaling relations (6) and (7) can be derived analytically (see Appendices B and C).

The relations $\tau_{\rm tp}(\epsilon) = (\Delta q)_{\rm tp}(\epsilon)/\epsilon$ and $\tau_{\rm rc}(\epsilon) = (\Delta q)_{\rm rc}(\epsilon)/\epsilon$ lead to the following algebraic scaling of the transient tipping and recovery times:

$$\tau_{\rm tp}(\epsilon) \sim \begin{cases} \epsilon^{\beta_{\rm tp}-1}, & \epsilon > \epsilon_c, \\ \epsilon^{-1}, & \epsilon < \epsilon_c, \end{cases} \tag{8}$$

$$\tau_{\rm rc}(\epsilon) \sim \begin{cases} \text{constant}, & \epsilon > \epsilon_c, \\ \epsilon^{-1}, & \epsilon < \epsilon_c, \end{cases} \tag{9}$$

as exemplified in Figs. 3(c) and 3(d), respectively. Note that, for $\epsilon \gg \epsilon_c$, the transient recovery time $\tau_{\rm rc}(\epsilon)$ approaches a constant.

4. Discussion

To summarize, we have uncovered a type of tipping behavior in a class nonautonomous nonsmooth biophysical systems that is quite distinct from the conventional tipping so far reported in the literature. Such a system describes the evolution of common skin diseases with different clinically distinguishable stages. The main feature of the unconventional tipping is that the transition from a high to a low stable steady state occurs through an intermediate oscillatory state in an extended duration of parameter changes or time. A similar scenario arises during the recovery process from the low to the high steady state. As a result, tipping and recovery are no longer "instantaneous" but transient, and the hysteresis loop exhibits a wrinkled structure. The clinical significance of these phenomena are the following. Given that transition from the high steady state to the intermediate oscillatory state corresponds to a sudden deterioration of the skin barrier with alternating symptoms and a further transition to the low state marks the onset of severe skin disease, the emergence of the intermediate state presents an opportunity for control intervention to prevent a healthy system from collapsing completely into the diseased state. Nonsmooth dynamics arise in biological and physical systems. Our findings indicate that tipping and hysteresis loop can manifest themselves in ways that have not been previously recognized.

The origin of the non-smoothness in the AD system is the various biological switches in the vector field, which represent a mathematical way to describe non-differentiable or discontinuous functions. In general, the governing equations of nonsmooth dynamical systems contain such functions. This often occurs due to effects such as impacts, friction, or switching behaviors in diverse physical and biological systems where sudden changes or interactions take place. Switches represent only a convenient way to describe nonsmooth systems. While the mathematical forms of the governing functions may differ from system to system, the generic feature of non-differentiability or discontinuity is shared by all nonsmooth dynamical systems. As demonstrated, nonsmooth systems are connected to real-world situations and they can exhibit unconventional phenomena that do not arise in smooth dynamical systems. Developing a rigorous mathematical theory to fully understand these unconventional behaviors in nonsmooth dynamical systems is challenging, but our physical and intuitive reasoning suggests the generality of the uncovered unconventional tipping phenomenon.

CRediT authorship contribution statement

Yoseb Kang: Writing – review & editing, Writing – original draft, Methodology, Investigation, Formal analysis, Data curation, Conceptualization. **Sangil Kim:** Writing – original draft, Supervision, Project administration, Conceptualization. **Ying-Cheng Lai:** Writing – review & editing, Writing – original draft, Supervision, Project administration, Formal analysis, Conceptualization. **Younghae Do:** Writing – review & editing, Writing – original draft, Supervision, Resources, Project administration, Investigation, Funding acquisition, Formal analysis, Conceptualization.

Declaration of competing interest

The authors declare that they have no known competing financial interests or personal relationships that could have appeared to influence the work reported in this paper.

Acknowledgments

This work was supported by the National Research Foundation of Korea, South Korea through Grants Nos. NRF-2022R1A5A1033624, NRF-2022R1A2C3011711, and by Global-Learning & Academic research institution for Master's·Ph.D. students, and Postdocs (LAMP) Program of the National Research Foundation of Korea grant funded by the Ministry of Education (No. RS-2023-00301938). The work at Arizona State University was supported by AFOSR, United States through Grant No. FA9550-21-1-0438.

Appendix A. Parameters of AD model

The parameter values of the AD system, Eq. (1), are described in Table A.1.

Appendix B. Scaling of tipping parameter interval and transient tipping time

We consider the tipping point associated with forward parameter ramping: $\kappa_p(t) = \kappa_p^s + \epsilon t$ (for $\epsilon > 0$ and $\kappa_p^s \ll b_1$). For $t > t_0 = 0$, the AD system approaches the fixed point H:

$$H = (P_1, B_1, D_1) = \left(\frac{P_{\text{env}}\kappa_p}{\delta_p(1+\gamma_B)}, 1, 0 \right). \tag{B.1}$$

From the existence condition of this fixed point [28], we get

$$\kappa_p \leq \kappa_p^c \equiv \frac{P^+\delta_p(1+\gamma_B)}{P_{\text{env}}}. \tag{B.2}$$

Table A.1
Description and values of parameters of the AD system.

Parameter	Description	Value
P_{env}	Environmental stress load	95 (mg/mL)
γ_B	Barrier-mediated inhibition of pathogen infiltration	1
κ_p	Nominal skin permeability	(1/day)
α_I	Rate of pathogen eradication by innate immune responses	(1/day)
δ_P	Basal pathogen death rate	1 (1/day)
κ_B	Barrier production rate	0.5 (1/day)
γ_R	Innate immunity-mediated inhibition of barrier production	10
δ_B	Rate of kallikrein-dependent barrier degradation	0.1
γ_G	Adaptive immunity-mediated inhibition of barrier production	1
κ_D	Rate of DC activation by receptors	4 cells/(mL 3 day)
δ_D	Rate of DC degradation	0.5 (1/day)
P^-	Receptor inactivation threshold	26.6 (mg/mL)
P^+	Receptor activation threshold	40 (mg/mL)
D^+	*Gata*3 activation threshold	85 (cells/mL)
R_{off}	Receptor off level	0
R_{on}	Receptor on level	16.7
G_{off}	*Gata*3 off level	0
G_{on}	*Gata*3 on level	1
K_{off}	Kallikrein off level	0
m_{on}	Slope of the linear relation between $P(t)$ and K_{on}	0.45
β_{on}	Y-intercept of the linear relation between $P(t)$ and K_{on}	6.71

When κ_p arrives at the bifurcating point b_1 at time t_1, i.e., $\kappa_p(t_1) = \kappa_p^c$ as shown in Fig. 1(b), all switches of AD system are off and $B(t) = 1$. In this case, the system is described by

$$\frac{dP}{dt} = \frac{P_{\text{env}}}{1+\gamma_B}\kappa_p(t) - \delta_p P(t), \tag{B.3}$$

which constitutes one of the subsystems of the AD system - the healthy subsystem whose solution can be obtained explicitly:

$$\begin{aligned} P(t) \;=\; & \frac{P_{\text{env}}}{\delta_p(1+\gamma_B)}\kappa_p(t) - \frac{P_{\text{env}}\epsilon}{\delta_p^2(1+\gamma_B)} \\ & + \left(P_0 - \frac{P_{\text{env}}\kappa_p^s}{\delta_p(1+\gamma_B)} + \frac{P_{\text{env}}\epsilon}{\delta_p^2(1+\gamma_B)}\right)e^{-\delta_p t}, \end{aligned} \tag{B.4}$$

where $P(0) = P_0$. For $t = t_1$, the third term in Eq. (B.4) becomes negligibly small. We get

$$P(t_1) = P^+ - \frac{P_{\text{env}}\epsilon}{\delta_p^2(1+\gamma_B)} + \mathcal{O} \lesssim P^+, \tag{B.5}$$

which causes the tipping point to be delayed. For $t > t_1$ and $P(t) \geq P^+$, the switches R and K are turned on, so the system equation becomes

$$\frac{dP}{dt} = \frac{P_{\text{env}}\kappa_p}{1+\gamma_B B(t)} - \alpha_I R_{\text{on}} P(t) - \delta_p P(t). \tag{B.6}$$

Using $P(t)$ in Eq. (B.4), we can find a time t_2 such that $P(t_2) = P^+$ or $\kappa_p(t_2) = q_1$. Since Eq. (B.4) contains the t and e^t terms, we use the Lambert W-function [84] to get a closed-form solution for t_2. Note that, in general, the Lambert W-function provides a method for solving equations of the form:

$$x = W(x)e^{W(x)}. \tag{B.7}$$

In our case, by expressing $P(t_2) = P^+$ and isolating the exponential term, we get

$$P^+ = A_1 + A_2 t_2 + A_3 e^{-\delta_P t_2}, \tag{B.8}$$

where

$$A_1 = \frac{P_{\text{env}}\kappa_p^s}{\delta_P(1+\gamma_B)} - \frac{P_{\text{env}}\epsilon}{\delta_P^2(1+\gamma_B)},$$

$$A_2 = \frac{P_{\text{env}}\epsilon}{\delta_P(1+\gamma_B)},$$
$$A_3 = P_0 - A_1.$$

Reparametrization gives

$$\mathcal{V} = \delta_P t_2 - \frac{\delta_P(P^+ - A_1)}{A_2}, \tag{B.9}$$

so the A_3 term in Eq. (B.8) can be expressed as

$$\begin{aligned} A_3 &= (P^+ - A_1 - A_2 t_2)e^{\delta_P t_2} \\ &= \left[P^+ - A_1 - A_2\frac{A_2\mathcal{V} + \delta_P(P^+ - A_1)}{\delta_P A_2}\right] e^{\mathcal{V} + \frac{\delta_P(P^+-A_1)}{A_2}} \\ &= -\frac{A_2}{\delta_P} e^{\frac{\delta_P(P^+-A_1)}{A_2}} \mathcal{V} e^{\mathcal{V}}. \end{aligned} \tag{B.10}$$

Using Eq. (B.10), we finally get

$$\frac{-A_3\delta_P}{A_2 \exp\dfrac{\delta_P(P^+ - A_1)}{A_2}} = \mathcal{V} e^{\mathcal{V}}. \tag{B.11}$$

Using the Lambert-W function, we obtain

$$\mathcal{V} = W_0\left[\frac{-\delta_P A_3}{A_2 \exp\dfrac{\delta_P(P^+ - A_1)}{A_2}}\right], \tag{B.12}$$

where W_0 is the principal branch of the Lambert W-function. From Eqs. (B.9) and (B.12), we can express t_2 as

$$t_2 = \frac{1}{\delta_P} W_0\left[\frac{-\delta_P A_3}{A_2 \exp\dfrac{\delta_P(P^+ - A_1)}{A_2}}\right] + \frac{P^+ - A_1}{A_2}. \tag{B.13}$$

Since the value of the Lambert W-function is small, i.e.,

$$W_0\left[\frac{-\delta_P A_3}{A_2 \exp\left(\frac{\delta_P(P^+-A_1)}{A_2}\right)}\right] \approx 0,$$

we have

$$t_2 \sim \frac{P^+ - A_1}{A_2} = \frac{\delta_P P^+(1+\gamma_B) - P_{\text{env}}\kappa_p^s}{P_{\text{env}}\epsilon} + \frac{1}{\delta_P}, \tag{B.14}$$

which implies

$$\begin{aligned} q_1 &= \kappa_p^s + \epsilon t_2 \\ &\sim \kappa_p^s + \epsilon\left(\frac{\delta_P(1+\gamma_B)P^+ - P_{\text{env}}\kappa_p^s}{P_{\text{env}}\epsilon} + \frac{1}{\delta_P}\right) \\ &= \frac{P^+\delta_P(1+\gamma_B)}{P_{\text{env}}} + \frac{\epsilon}{\delta_P} \end{aligned} \tag{B.15}$$

Using Eq. (B.2), we get

$$\begin{aligned} q_1 - b_1 &= \kappa_p(t_2) - \kappa_p(t_1) \\ &\sim \left(\frac{P^+\delta_P(1+\gamma_B)}{P_{\text{env}}} + \frac{\epsilon}{\delta_P}\right) - \frac{P^+\delta_p(1+\gamma_B)}{P_{\text{env}}} \\ &= \frac{\epsilon}{\delta_P} \sim \epsilon, \end{aligned} \tag{B.16}$$

which gives the effect of the parameter changing rate on the delay of the first tipping point.

Calculating the tipping parameter interval $(\Delta q)_{\text{tp}} \equiv q_2 - q_1$ requires the quantity $q_2 - b_1$, where $q_2 = \kappa_p(t_3)$. The system exhibits oscillatory dynamics between q_1 and q_2. With the aid of the slope function F_i^s introduced in Ref. [29], the oscillating behavior

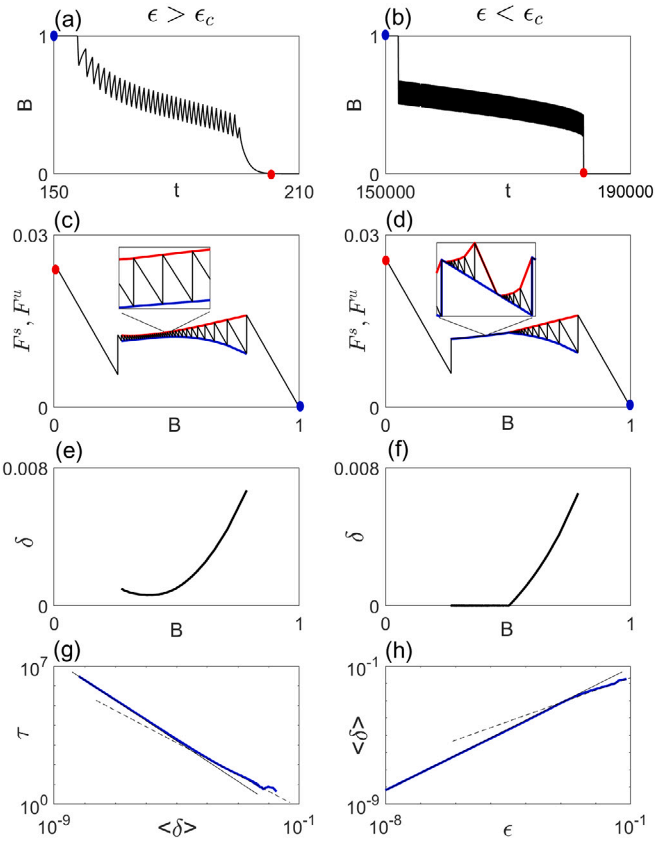

Fig. B.4. Transformed dynamics of tipping associated with different forward ramping rates ϵ. (a, b) Tipping points and change of AD states for $\epsilon = 10^{-3}$ and 10^{-6}, respectively. (c, d) The transformed tipping trajectories in (a, b), respectively. Red and Blue dots indicate the chronic damage (C) and healthy recovery (H), respectively, while the red and blue curves represent a nonsmooth opened channel created by the slope functions, F^s and F^u (magnified). (e,f) Heights of the opened channels in (c, d), respectively. (g) Algebraic scaling of the escaping time τ, where the scaling exponents are indicated by the solid and dotted lines, as represented by Eq. (B.17). (h) The relation between the average height $\langle\delta\rangle$ and the ramping speed ϵ, as represented by Eq. (B.18). (For interpretation of the references to color in this figure legend, the reader is referred to the web version of this article.)

can be understood as a type of transient dynamics induced by an open dynamical channel. For instance, Figs. B.4(a–d) show the transformed behavior for the occurrence of the second tipping point for two different values of the ramping rate. In particular, a trajectory's passing through the open channel gives rise to the second tipping point and the associated transient behavior [29].

To determine the transient tipping time τ through the open channel marked by the red and blue curves in Figs. B.4(c, d) [or the transient tipping time τ from b_1 to q_2 in Figs. B.4(a, b)], we examine the height of the open channel created by the two underlying slope functions, specifically, the height between the red and blue curves as illustrated in Figs. B.5(c–d). The average height $\langle\delta\rangle$ of the open channel in Figs. B.5(e–f) can then be calculated. Since the AD system is nonsmooth, the curves defining the channel are irregular with a kink structure, as shown in Figs. B.4(c, d). For each ramping rate ϵ, we numerically obtain the following scaling law for τ:

$$\tau \sim \begin{cases} \langle\delta\rangle^{c_1}, & \epsilon > \epsilon_c, \\ \langle\delta\rangle^{c_2}, & \epsilon < \epsilon_c, \end{cases} \tag{B.17}$$

where $c_1 \approx -0.74$ and $c_2 \approx -1$ [from Fig. B.4(g)]. Since the channel height depends on the ramping speed ϵ as

$$\langle\delta\rangle \sim \begin{cases} \epsilon^{d_1}, & \epsilon > \epsilon_c, \\ \epsilon^{d_2}, & \epsilon < \epsilon_c, \end{cases} \tag{B.18}$$

where $d_1 \approx 0.5$ and $d_2 \approx 1$ [Fig. B.4(h)], we obtain

$$\begin{aligned} q_2 - b_1 &= \kappa_p(t_3) - \kappa_p(t_1) = \epsilon(t_3 - t_1) \sim \epsilon\tau \\ &\sim \begin{cases} \epsilon^{1+c_1 d_1} & \epsilon > \epsilon_c, \\ \text{constant} & \epsilon < \epsilon_c. \end{cases} \end{aligned} \tag{B.19}$$

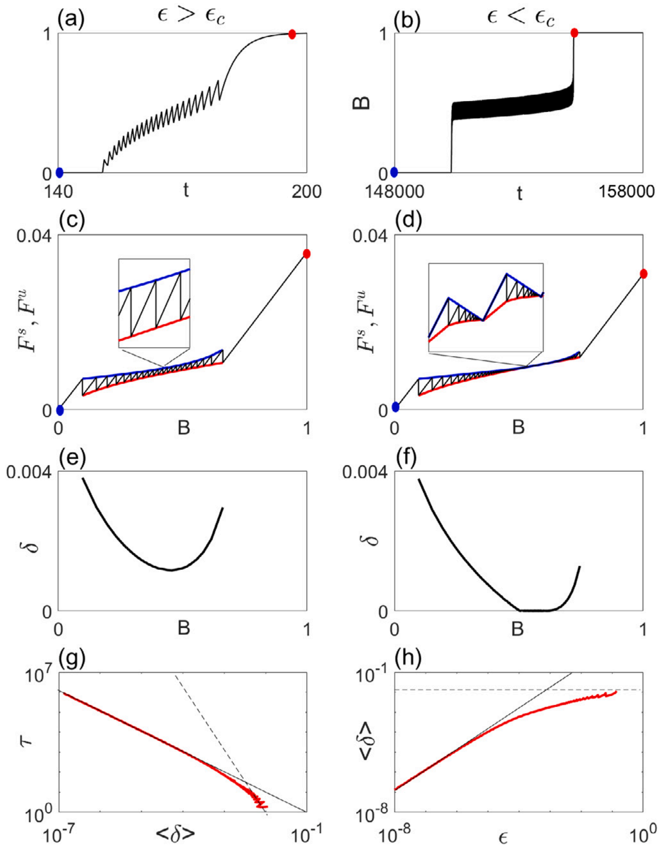

Fig. B.5. Transformed dynamics of recovery points for different parameter ramping rate. The legends are the same as in Fig. B.4.

Let $\beta_{\mathrm{tp}} \equiv 1 + c_1 d_1 \approx 2/3$. For $\epsilon \to 0$, the AD system becomes stationary, so the constant is the distance between the two bifurcation points $b_2 - b_1$. Combining Eqs. (B.16) and (B.19), we get

$$(\Delta q)_{\mathrm{tp}}(\epsilon) = q_2 - q_1 \sim \begin{cases} \epsilon^{\beta_{\mathrm{tp}}} - \epsilon, & \epsilon > \epsilon_c, \\ b_2 - b_1 - \epsilon, & \epsilon < \epsilon_c. \end{cases}$$

For $\epsilon < \epsilon_c$, we have $(b_2 - b_1 - \epsilon)/(b_2 - b_1) \approx 1$ due to the smallness of ϵ. For $\epsilon > \epsilon_c$, we get

$$1 > \frac{\epsilon^{\beta_{\mathrm{tp}}} - \epsilon}{\epsilon^{\beta_{\mathrm{tp}}}} = 1 - \epsilon^{1-\beta_{\mathrm{tp}}} > 1 - \epsilon_c^{1-\beta_{\mathrm{tp}}} = \mathrm{constant}.$$

It implies that $\epsilon^{\beta_{\mathrm{tp}}} > \epsilon^{\beta_{\mathrm{tp}}} - \epsilon > \mathrm{Constant} \times \epsilon^{\beta_{\mathrm{tp}}}$. Finally, we have

$$(\Delta q)_{\mathrm{tp}}(\epsilon) \sim \begin{cases} \epsilon^{\beta_{\mathrm{tp}}}, & \epsilon > \epsilon_c, \\ b_2 - b_1, & \epsilon < \epsilon_c, \end{cases}$$

as shown in Fig. 3(a). The relation $\tau_{\mathrm{tp}}(\epsilon) = (\Delta q)_{\mathrm{tp}}(\epsilon)/\epsilon$ leads to the following algebraic scaling of the transient tipping time:

$$\tau_{\mathrm{tp}}(\epsilon) \sim \begin{cases} \epsilon^{\beta_{\mathrm{tp}}-1}, & \epsilon > \epsilon_c, \\ \epsilon^{-1}, & \epsilon < \epsilon_c, \end{cases} \tag{B.20}$$

Appendix C. Scaling of recovery parameter interval and transient recovery time

We consider the recovery scenario where the bifurcation parameter changes in the opposite (backward) direction: $\kappa_p(t) = \kappa_p^s - \epsilon t$ for $\epsilon > 0$ and $\kappa_p^s \gg b_3$. For $t > t_0 = 0$, the AD system come close to the steady state of chronic damage characterized by the fixed point $C = (P_4, B_4, D_4)$ given by

$$P_4 = \frac{P_{\mathrm{env}} \kappa_p}{(\alpha_I R_{\mathrm{on}} + \delta_p)(1 + \gamma_B B_4)}$$

$$B_4 = \frac{\kappa_B}{\delta_B (m_{on} P_4 - \beta)(1 + \gamma_R R_{\mathrm{on}})(1 + \gamma_G G_{on})} \tag{C.1}$$

$$D_4 = \frac{\kappa_D R_{\rm on}}{\delta_D}.$$

The existence condition of this fixed point [28] gives

$$\kappa_p \geq \kappa_p^c \equiv \frac{P^-(\alpha_I R_{\rm on} + \delta_P)(1+\gamma_B B_4)}{P_{\rm env}}. \tag{C.2}$$

As κ_p reaches the bifurcating point b_3 at time t_4 determined by $\kappa_p(t_4) = \kappa_p^c$ [see Fig. 1(b)], all switches of the AD system are on and the value of $B(t)$ is near zero: $B(t) = B^* \sim 0$. In this case, the AD system, Eq. (1), can be rewritten as

$$\frac{dP}{dt} = \frac{P_{\rm env}}{1+\gamma_B B^*}\kappa_p(t) - (\alpha_I R_{\rm on} + \delta_p)P(t), \tag{C.3}$$

whose solution is

$$\begin{aligned} P(t) = & \frac{P_{\rm env}\kappa_p(t)}{(\alpha_I R_{\rm on} + \delta_p)(1+\gamma_B B^*)} + \frac{P_{\rm env}\epsilon}{(\alpha_I R_{\rm on} + \delta_p)^2(1+\gamma_B B^*)} \\ & + \left(P_0 - \frac{P_{\rm env}\kappa_p^s}{(\alpha_I R_{\rm on} + \delta_p)(1+\gamma_B)}\right. \\ & \left. - \frac{P_{\rm env}\epsilon}{(\alpha_I R_{\rm on} + \delta_p)^2(1+\gamma_B)}\right) e^{-(\alpha_I R_{\rm on}+\delta_p)t}, \end{aligned}$$

where $P(0) = P_0$. From a direct computation of $P(t_4)$, we obtain

$$P(t_4) = P^- + \frac{P_{\rm env}\epsilon}{(\alpha_I R_{\rm on} + \delta_p)^2(1+\gamma_B B^*)} + \mathcal{O} \gtrsim P^-,$$

leading to a delay effect, where $\kappa_p(t_4) = b_3$.

For $t > t_4$ defined by $P(t) \leq P^-$, the switches R and K of the system are off, so the system equation becomes

$$\frac{dP}{dt} = \frac{P_{\rm env}\kappa_p}{1+\gamma_B B(t)} - \delta_p P(t). \tag{C.4}$$

At $t = t_5$ determined by $P(t_5) = P^-$, the first tipping point occurs: $q_3 = \kappa_p(t_5)$. Similar to the analysis in Appendix B, t_5 can be found by using the Lambert W-function:

$$t_5 = \frac{1}{A_7} W_0\left[\frac{A_6 A_7}{A_5}\exp\frac{A_7(P^- - A_4)}{A_5}\right] - \frac{P^- - A_4}{A_5}, \tag{C.5}$$

where

$$\begin{aligned} A_4 &= \frac{P_{\rm env}\kappa_p^s}{(\alpha_I R_{\rm on} + \delta_p)(1+\gamma_B B^*)} - \frac{P_{\rm env}\epsilon}{(\alpha_I R_{\rm on} + \delta_p)^2(1+\gamma_B B^*)}, \\ A_5 &= \frac{P_{\rm env}\epsilon}{(\alpha_I R_{\rm on} + \delta_p)(1+\gamma_B B^*)}, \\ A_6 &= P_0 - A, \\ A_7 &= \alpha_I R_{\rm on} + \delta_p. \end{aligned}$$

Using the property of the Lambert W-function, t_5 can be approximated as

$$\begin{aligned} t_5 &\sim -\frac{P^- - A_4}{A_5} \\ &= \frac{1}{\alpha_I R_{\rm on} + \delta_P} \\ &\quad + \frac{P_{\rm env}\kappa_p^s - P^-(\alpha_I R_{\rm on} + \delta_P)(1+\gamma_B B^*)}{P_{\rm env}} \cdot \frac{1}{\epsilon}, \end{aligned} \tag{C.6}$$

leading to

$$\begin{aligned} q_3 &= \kappa_p^s - \epsilon t_5 \\ &\sim \frac{P^-(\alpha_I R_{\rm on} + \delta_P)(1+\gamma_B B_4)}{P_{\rm env}} - \frac{\epsilon}{\alpha_I R_{\rm on} + \delta_P} \\ &= b_3 - \frac{\epsilon}{\alpha_I R_{\rm on} + \delta_P}. \end{aligned} \tag{C.7}$$

As a result, we get

$$b_3 - q_3 = b_3 - (b_3 - \frac{\epsilon}{\alpha_I R_{\text{on}} + \delta_P}) = \frac{\epsilon}{\alpha_I R_{\text{on}} + \delta_P} \sim \epsilon, \tag{C.8}$$

which gives the first recovery point.

The scaling of the second recovery can also be obtained in a similar way to that of the tipping (forward) case. The transient recovery time τ from b_3 to q_4 can be numerically obtained as

$$\tau \sim \begin{cases} \langle\delta\rangle^{c_1}, & \epsilon > \epsilon_c, \\ \langle\delta\rangle^{c_2}, & \epsilon < \epsilon_c, \end{cases} \tag{C.9}$$

where $c_1 \approx -3$ and $c_2 \approx -1$ [Fig. B.5(g)]. The height associated with the ramping rate ϵ is

$$\langle\delta\rangle \sim \begin{cases} \epsilon^{d_1}, & \epsilon > \epsilon_c, \\ \epsilon^{d_2}, & \epsilon < \epsilon_c, \end{cases} \tag{C.10}$$

where $d_1 \to 0$ as ϵ grows and $d_2 \approx 1$ [Fig. B.5(h)]. We obtain

$$\begin{aligned} b_3 - q_4 &= \kappa_p(t_4) - \kappa_p(t_6) = \epsilon(t_6 - t_4) \\ &\sim \epsilon\tau \\ &\sim \begin{cases} \epsilon^{1+c_1 d_1}, & \epsilon > \epsilon_c, \\ \epsilon^{1+c_2 d_2}, & \epsilon < \epsilon_c, \end{cases} \\ &\sim \begin{cases} \epsilon^{1+c_1 d_1}, & \epsilon > \epsilon_c, \\ \text{constant}, & \epsilon < \epsilon_c, \end{cases} \end{aligned} \tag{C.11}$$

because $c_2 d_2 = -1$. Let $\beta_{\text{rc}} \equiv 1 + c_1 d_1 \approx 1$. For $\epsilon \to 0$, the system becomes stationary, so the constant is the distance $b_3 - b_4$ between the two bifurcation points. Using Eqs. (C.8) and (C.11), we obtain

$$\begin{aligned} (\Delta q)_{\text{rc}}(\epsilon) &= q_3 - q_4 \\ &\sim \begin{cases} \epsilon^{\beta_{\text{rc}}} - \epsilon, & \epsilon > \epsilon_c, \\ b_3 - b_4 - \epsilon, & \epsilon < \epsilon_c, \end{cases} \\ &\sim \begin{cases} \epsilon^{\beta_{\text{rc}}}, & \epsilon > \epsilon_c, \\ b_3 - b_4, & \epsilon < \epsilon_c, \end{cases} \end{aligned}$$

as shown in Fig. 3(b). The relation

$$\tau_{\text{rc}}(\epsilon) = (\Delta q)_{\text{rc}}(\epsilon)/\epsilon$$

leads to the following algebraic scaling of the transient tipping and recovery times:

$$\tau_{\text{rc}}(\epsilon) \sim \begin{cases} \text{constant}, & \epsilon > \epsilon_c, \\ \epsilon^{-1}, & \epsilon < \epsilon_c. \end{cases} \tag{C.12}$$

Data availability

No data was used for the research described in the article.

References

[1] Glass L, Mackey MC. From clocks to chaos: the rhythms of life. Princeton, NJ: Princeton University Press; 1988.
[2] Kaplan D, Glass L. Understanding nonlinear dynamics. Berlin: Springer-Verlag; 1995.
[3] Mackey MC, Glass L. Oscillation and chaos in physiological control systems. Science 1977;197(4300):287–9.
[4] Glass L, Mackey MC. Pathological conditions resulting from instabilities in physiological control systems. Ann New York Acad Sci 1979;316(1):214–35.
[5] Belair J, Glass L, an der Heiden U, Milton J. Dynamical disease: Identification, temporal aspects and treatment strategies for human illness. Chaos 1995;5(1):1–7.
[6] Milton J, Jung P. Epilepsy as a dynamic disease. New York: Springer; 2003.
[7] Osorio I, Frei MG, Sornette D, Milton J, Lai Y-C. Epileptic seizures: Quakes of the brain? Phys Rev E 2010;82:021919.
[8] Lai Y-C, Harrison MAF, Frei MG, Osorio I. Inability of Lyapunov exponents to predict epileptic seizures. Phys Rev Lett 2003;91:068102.
[9] Lai Y-C, Harrison MAF, Frei MG, Osorio I. Controlled test for predictive power of Lyapunov exponents: Their inability to predict epileptic seizures. Chaos 2004;14:630–42.
[10] Harrison MAF, Osorio I, Frei MG, Asuri S, Lai Y-C. Correlation dimension and integral do not predict epileptic seizures. Chaos 2005;15:033106.
[11] Lai Y-C, Frei MG, Osorio I, Huang L. Characterization of synchrony with applications to epileptic brain signals. Phys Rev Lett 2007;98:108102.
[12] Leung DYM. Pathogenesis of atopic dermatitis. J Allergy Clin Immunol 1999;104(3):S99–108.
[13] Furue M, Yamazaki S, Jimbow K, Tsuchida T, Amagai M, Tanaka T, et al. Prevalence of dermatological disorders in Japan: a nationwide, cross-sectional, seasonal, multicenter, hospital-based study. J Dermatol 2011;38(4):310–20.
[14] Leung DY. Atopic dermatitis: new insights and opportunities for therapeutic intervention. J Allergy Clin Immunol 2000;105:860.
[15] Bieber T, De Angelo M, Akdis CA, Traidl-Hoffmann C, Lauener R, Schäppi G, et al. Clinical phenotypes and endophenotypes of atopic dermatitis: Where are we, and where should we go? J Allergy Clin Immunol 2017;139(4):S58–64.

[16] Yew YW, Thyssen JP, Silverberg JI. A systematic review and meta-analysis of the regional and age-related differences in atopic dermatitis clinical characteristics. J Am Acad Dermatol 2019;80:390–401.
[17] Kim YJ, Yun SJ, Lee J-B, Kim SJ, Won YH, Lee S-C. Four years prospective study of natural history of atopic dermatitis aged 7˜ 8 years at an individual level: a community-based survey by dermatologists' skin examination in childhood. Ann Dermatol 2016;28:684.
[18] Illi S, von Mutius E, Lau S, Nickel R, Grüber C, Niggemann B, et al. The natural course of atopic dermatitis from birth to age 7 years and the association with asthma. J Allergy Clin Immunol 2004;113:925.
[19] Roduit C, Frei R, Depner M, Karvonen AM, Renz H, Braun-Fahrländer C, et al. Phenotypes of atopic dermatitis depending on the timing of onset and progression in childhood. JAMA Pediatr 2017;171(7):655–62.
[20] Vakirlis E, Lazaridou E, Tzellos TG, Gerou S, Chatzidimitriou D, Ioannides D. Investigation of cytokine levels and their association with SCORAD index in adults with acute atopic dermatitis. J Euro. Acad Dermatol Venereol 2011;25(4):409–16.
[21] Garmhausen D, Hagemann T, Bieber T, Dimitriou I, Fimmers R, Diepgen T, et al. Characterization of different courses of atopic dermatitis in adolescent and adult patients. Allergy 2013;68:498.
[22] Abuabara K, Margolis DJ, Langan SM. The long-term course of atopic dermatitis. Dermatol Clin 2017;35:291.
[23] Tanaka RJ, Ono M. Skin disease modeling from a mathematical perspective. J Invest Dermatol 2013;133:1472.
[24] Eyerich K, Brown SJ, White BEP, Tanaka RJ, Bissonette R, Dhar S, et al. Human and computational models of atopic dermatitis: A review and perspectives by an expert panel of the international eczema council. J Allergy Clin Immunol 2019;143:36.
[25] Christodoulides P, Hirata Y, Domínguez-Hüttinger E, Danby SG, Cork MJ, Williams HC, et al. Computational design of treatment strategies for proactive therapy on atopic dermatitis using optimal control theory. Philos Trans R. Soc A 2017;375:20160285.
[26] Domínguez-Hüttinger E, Christodoulides P, Miyauchi K, Irvine AD, Okada-Hatakeyama M, Kubo M, et al. Mathematical modeling of atopic dermatitis reveals double-switch mechanisms underlying 4 common disease phenotypes. J Allergy Clin Immunol 2017;139:1861.
[27] Tanaka G, Domínguez-Hüttinger E, Christodoulides P, Aihara K, Tanaka RJ. Bifurcation analysis of a mathematical model of atopic dermatitis to determine patient-specific effects of treatments on dynamic phenotypes. J Theoret Biol 2018;448:66.
[28] Kang Y, Lee EH, Kim S, Jang YH, Do Y. Complexity and multistability of a nonsmooth atopic dermatitis system. Chaos Solitons Fractals 2021;153:111575.
[29] Kang Y, Hwang J, Lai Y-C, Choi H, Do Y. A nonlinear transient-dynamics approach to atopic dermatitis: Role of spontaneous remission. Chaos Solitons Fractals 2024;179:114464.
[30] Angeli D, Ferrell J, Sontag ED. Detection of multistability, bifurcations, and hysteresis in a large class of biological positive-feedback systems. Proc Nat Acad Sci (USA) 2004;101:1822.
[31] Umulis DM, Serpe M, O'Connor MBO, Othmer HG. Robust, bistable patterning of the dorsal surface of the drosophila embryo. Proc Nat Acad Sci (USA) 2006;103:11613.
[32] Wu M, Su R-Q, Li X-H, Ellis T, Lai Y-C, Wang X. Engineering of regulated stochastic cell fate determination. Proc Nat Acad Sci (USA) 2013;110:10610.
[33] Wang L-Z, Su R-Q, Huang Z-G, Wang X, Wang W-X, Grebogi C, et al. A geometrical approach to control and controllability of nonlinear dynamical networks. Nat Commun 2016;7:11323.
[34] Wu F-Q, Su R-Q, Lai Y-C, Wang X. Engineering of a synthetic quadrastable gene network to approach Waddington landscape and cell fate determination. ELife 2017;6:e23702.
[35] Argyropoulos C, Chen P-Y, Monticone F, D'Aguanno G, Alù A. Nonlinear plasmonic cloaks to realize giant all-optical scattering switching. Phys Rev Lett 2012;108:263905.
[36] Sheng J, Khadka U, Xiao M. Realization of all-optical multistate switching in an atomic coherent medium. Phys Rev Lett 2012;109:223906.
[37] Andersen CK, Mølmer K. Circuit qed flip-flop memory with all-microwave switching. Phys Rev Appl 2015;3:024002.
[38] Bacot V, Perrard S, Labousse M, Couder Y, Fort E. Multistable free states of an active particle from a coherent memory dynamics. Phys Rev Lett 2019;122:104303.
[39] Winters D, Abeed MA, Sahoo S, Barman A, Bandyopadhyay S. Reliability of magnetoelastic switching of nonideal nanomagnets with defects: A case study for the viability of straintronic logic and memory. Phys Rev Appl 2019;12:034010.
[40] Fermin R, Scheinowitz NMA, Aarts J, Lahabi K. Mesoscopic superconducting memory based on bistable magnetic textures. Phys Rev Res 2022;4:033136.
[41] Bi M-X, Fan H, Yan X-H, Lai Y-C. Folding state within a hysteresis loop: Hidden multistability in nonlinear physical systems. Phys Rev Lett 2024;132:137201.
[42] Scheffer M. In: Critical transitions in nature and society, vol. 16, Princeton Univ. Press; 2020.
[43] Scheffer M. Ecology of shallow lakes. Springer; 2004.
[44] Boettiger C, Hastings A. Tipping points: From patterns to predictions. Nature 2013;493:157.
[45] Scheffer M, Bascompte J, Brock WA, Brovkin V, Carpenter SR, Dakos V, et al. Early-warning signals for critical transitions. Nature 2009;461:53.
[46] Scheffer M. Complex systems: foreseeing tipping points. Nature 2010;467:411.
[47] Wysham DB, Hastings A. Regime shifts in ecological systems can occur with no warning. Ecol Lett 2010;13:464.
[48] Drake JM, Griffen BD. Early warning signals of extinction in deteriorating environments. Nature 2010;467:456.
[49] Boettiger C, Hastings A. Quantifying limits to detection of early warning for critical transitions. J R. Soc Interface 2012;9:2527.
[50] Dai L, Vorselen D, Korolev KS, Gore J. Generic indicators for loss of resilience before a tipping point leading to population collapse. Science 2012;336:1175.
[51] Tylianakis JM, Coux C. Tipping points in ecological networks. Trends Plant Sci 2014;19:281.
[52] Lever JJ, Nes EH, Scheffer M, Bascompte J. The sudden collapse of pollinator communities. Ecol Lett 2014;17:350.
[53] Gualdia S, Tarziaa M, Zamponic F, Bouchaudd J-P. Tipping points in macroeconomic agent-based models. J Econom Dynam Control 2015;50:29.
[54] Jiang J, Huang Z-G, Seager TP, Lin W, Grebogi C, Hastings A, et al. Predicting tipping points in mutualistic networks through dimension reduction. Proc Nat Acad Sci (USA) 2018;115:E639.
[55] Jiang J, Hastings A, Lai Y-C. Harnessing tipping points in complex ecological networks. J R. Soc Interface 2019;16:20190345.
[56] Meng Y, Jiang J, Grebogi C, Lai Y-C. Noise-enabled species recovery in the aftermath of a tipping point. Phys Rev E 2020a;101:012206.
[57] Meng Y, Grebogi C. Control of tipping points in stochastic mutualistic complex networks. Chaos 2021;31:023118.
[58] Meng Y, Lai Y-C, Grebogi C. Tipping point and noise-induced transients in ecological networks. J R. Soc Interface 2020b;17:20200645.
[59] Meng Y, Lai Y-C, Grebogi C. The fundamental benefits of multiplexity in ecological networks. J R. Soc Interface 2022;19:20220438.
[60] O'Keeffe PE, Wieczorek S. Tipping phenomena and points of no return in ecosystems: Beyond classical bifurcations. SIAM J Appl Dyn Syst 2020;19:2371.
[61] Chen L, Liu R, Liu Z-P, et al. Detecting early-warning signals for sudden deterioration of complex diseases by dynamical network biomarkers. Sci Rep 2012;2:342.
[62] Yang B, Li M, Tang W, Liu S, Zhang Weixinand, Chen L, et al. Dynamic network biomarker indicates pulmonary metastasis at the tipping point of hepatocellular carcinoma. Nat Commun 2018;9:678.
[63] Thompson JMT, Sieber J. Predicting climate tipping as a noisy bifurcation: A review. Int J Bif. Chaos 2011;21(02):399–423.
[64] Ashwin P, Wieczorek S, Vitolo R, Cox P. Tipping points in open systems: bifurcation, noise-induced and rate-dependent examples in the climate system. Phil. Trans. R. Soc. A 2012;370:1166.
[65] Lenton TM, Livina VN, Dakos V, van Nes EH, Scheffer M. Early warning of climate tipping points from critical slowing down: comparing methods to improve robustness. Phil. Trans. R. Soc. A 2012;370:1185.
[66] Barnosky AD, Hadly EA, Bascompte J, Brown ELBJH, Fortelius M, Getz WM, et al. Approaching a state shift in earth's biosphere. Nature 2012;486:52.

[67] Lontzek TS, Cai Y-Y, Judd KL, Lenton TM. Stochastic integrated assessment of climate tipping points indicates the need for strict climate policy. Nat Clim Chang 2015;5:441.

[68] Buckley MW, Marshall J. Observations, inferences, and mechanisms of the Atlantic meridional overturning circulation: A review. Rev Geophys 2016;54:5.

[69] Trenberth KE, Zhang Y, Fasullo JT, Cheng L. Observation-based estimates of global and basin ocean meridional heat transport time series. J Clim 2019;32:4567.

[70] Jackson LC, Biastoch A, Buckley MW, Desbruyères DG, Frajka-Williams E, Moat B, et al. The evolution of the North Atlantic meridional overturning circulation since 1980. Nat Rev Earth Env 2022;3:241.

[71] Lohmann J, Ditlevsen PD. Risk of tipping the overturning circulation due to increasing rates of ice melt. Proc Natl Acad Sci (USA) 2021;118:e2017989118.

[72] Ditlevsen P, Ditlevsen S. Warning of a forthcoming collapse of the Atlantic meridional overturning circulation. Nat Commun 2023;14:4254.

[73] Panahi S, Kong L-W, Moradi M, Zhai Z-M, Glaz B, Haile M, et al. Machine learning prediction of tipping in complex dynamical systems. Phys Rev Res 2024;6:043194.

[74] Ashwin P, Perryman C, Wieczorek S. Parameter shifts for nonautonomous systems in low dimension: bifurcation-and rate-induced tipping. Nonlinearity 2017;30:2185.

[75] Vanselow A, Wieczorek S, Feudel U. When very slow is too fast-collapse of a predator–prey system. J Theoret Biol 2019;479:64.

[76] Synodinos AD, Karnatak R, Aguilar-Trigueros CA, Gras P, Heger T, Ionescu D, et al. The rate of environmental change as an important driver across scales in ecology. Oikos 2023;2023:e09616.

[77] Vanselow A, Halekotte L, Pal P, Wieczorek S, Feudel U. Rate-induced tipping can trigger plankton blooms. Theo. Ecol 2024;17:89.

[78] Feudel U. Rate-induced tipping in ecosystems and climate: the role of unstable states, basin boundaries and transient dynamics. Nonlinear Proc Geophys 2023;30:481.

[79] Panahi S, Do Y, Hastings A, Lai Y-C. Rate-induced tipping in complex high-dimensional ecological networks. Proc Nat Acad Sci (USA) 2023;120:e2308820120.

[80] Bending D, Ono M. Interplay between the skin barrier and immune cells in patients with atopic dermatitis unraveled by means of mathematical modeling. J Allergy Clin Immunol 2017;139:1790.

[81] Kang Y, Hwang J, Jang YH, Lai Y-C, Do Y. Inflammation dynamics of atopic dermatitis: Phase transition and scaling law of remission time. Comput Biol Med 2025;194:110391.

[82] Liao Y-H, Chen S-Y, Chou S-Y, Wang P-H, Tsai M-R, Sun C-K. Determination of chronological aging parameters in epidermal keratinocytes by in vivo harmonic generation microscopy. Biomed Opt Express 2013;4:77.

[83] Rübe CE, Bäumert C, Schuler N, Isermann A, Schmal Z, Glanemann M, et al. Human skin aging is associated with increased expression of the histone variant h2a. j in the epidermis. NPJ Aging. Mech Dis 2021;7:7.

[84] Corless RM, Gonnet GH, Hare DEG, Jeffrey DJ, Knuth DE. On the Lambert W function. Adv Comput Math 1996;5:329–59.